

# Smoothed Particle Hydrodynamics modeling of granular column collapse

**Kamil Szewc**

Received: date / Accepted: date

**Abstract** The Smoothed Particle Hydrodynamics (SPH) is a particle-based, Lagrangian method for fluid-flow simulations. In this work, fundamental concepts of this method are first briefly recalled. Then, the ability to accurately model granular materials using an introduced visco-plastic constitutive rheological model is studied. For this purpose sets of numerical calculations (2D and 3D) of the fundamental problem of the collapse of initially vertical cylinders of granular materials are performed. The results of modeling of columns with different aspect ratios and different angles of internal friction are presented. The numerical outcomes are assessed not only with respect to the reference experimental data but also with respect to other numerical methods, namely the Distinct Element Method and the Finite Element Method. In order to improve the numerical efficiency of the method, the Graphics Processing Units implementation is presented and some related issues are discussed. It is believed that this study corresponds to a new application of SPH approaches for simulations of granular media and results reveal the interest of this method to capture fine details of processes of such complex problems as waves-seabed interactions.

**Keywords** Granular flow · Lagrangian methods · Landslides

## 1 Introduction

Problems involving large granular media deformations are active research in the fields of geomechanics and natural hazard management. Particular atten-

---

K. Szewc  
Institute of Fluid-Flow Machinery  
Polish Academy of Sciences  
ul. Fiszerka 14  
80-231 Gdańsk  
E-mail: kszewc@imp.gda.pl

tion is paid to understand the processes and to learn how to predict the run-outs of rock and debris avalanches or landslides which can be very destructive. Therefore, the accurate modeling of such flows is invaluable.

In order to simulate flowing granular media, many researchers derived the semi-empirical depth-averaged models, see [1, 2, 3, 4, 5]. The main disadvantage of such models is inability to accurately model high but narrow stacks of granular materials. This drawback implied a need to develop more detailed computational models for granular material dynamics. One of the most widely used methods to simulate such problems is the Distinct Element Method (DEM) [6]. The first application of DEM to model granular flows was proposed in [7]. Further improvements have been described in [8, 9, 10, 11, 12]. Nowadays, the DEM method is widely accepted as an effective approach for modeling granular and discontinuous materials. Even though the DEM approach is computationally expensive, this approach is easy to be written in a parallel manner. Despite many advantages of DEM, there is one relevant disadvantage – this approach is designed to discrete materials modeling, therefore the introduction of a new physics can be very complex. For example, to model interactions of granular material with fluid-flow, the coupling with another CFD method is necessary. One of the alternative methods which allow to deal with multi-physics is the Finite Element Method (FEM), see [13] for details. To the best of our knowledge, the first application of FEM to model the granular material collapse was proposed in [14]. The authors used the continuum approach based on an elasto-plastic model. The main disadvantage of FEM is the grid-based nature of this method. When large deformations occur, the FEM approach suffers from grid distortions. However, in the last decade, many so-called meshless methods have been developed.

One of the most mature and commonly used approach is the Smoothed Particle Hydrodynamics method (SPH). In the early stage it was developed to simulate some astrophysical phenomena at the hydrodynamic level [15]. The main idea behind the SPH method is to introduce kernel interpolants for flow quantities in order to represent fluid dynamics by a set of particle evolution equations. Due to its Lagrangian nature, for multiphase flows, there is no necessity to handle (reconstruct or track) the interface shape as in the grid-based methods. Therefore, there is no additional numerical diffusion related to the interface handling. For this reason and the fact that the SPH approach is well suited to problems with large density differences, free-surfaces and complex geometries, the SPH method is increasingly used for hydro-engineering and geophysical applications, for review see [16, 17]. The first attempts to model the granular materials using the SPH approach was presented by *Bui et al. (2008)* [18, 19]. The authors decided to use an elasto-plastic (Drucker-Prager) constitutive model. Despite good results compared with the experimental and numerical data, authors reported a serious tensile instability problems. Another constitutive model was proposed by *Ulrich et al. 2013* [20], where the granular material is treated as a fluid with a variable viscosity (a visco-plastic rheological model), however, authors have not presented any validations of this approach.

In the present work, the ability to model granular materials using the SPH method and the visco-plastic model is studied. For this purpose, it was decided to perform a set of numerical calculations (in 2D and 3D) of the fundamental problem of the collapse of initially vertical cylinders of granular materials. The obtained results were compared with other numerical (DEM and FEM) and the experimental data. One of the drawbacks of the mesh-free methods is much lower numerical efficiency compared with the grid-based approaches. However, similarly to the DEM method, the SPH approach numerical implementations present a high degree of spatial data locality and significant number of independent calculations, therefore the code can be easily written in a massively parallel manner. In recent years new techniques allowing numerical simulations to be performed using Graphics Processing Units (GPU) have been developed. The massive parallel capability of modern GPUs allows simulations of large systems to be performed using cheap desktop computers. For the purpose of this study, it was decided to implement the SPH method using GPU programming techniques. Some issues related to the GPU computations are discussed.

The paper is organized as follows: in Section 2 the brief introduction to SPH is presented; in Section 3 the visco-plastic rheological model of granular materials is introduced; in Section 4 the implementation on GPU is discussed; then in Section 5 the obtained numerical results are presented. In order to validate the model, the following criteria are taken into account: the granular deposit evolution (Section 5.2), run-out distances (Section 5.3), the energy contribution (Section 5.4) and the inclination of the failure plane (Section 5.5). The numerical efficiency is discussed in Section 5.6.

## 2 SPH formulation

The full set of governing equations for incompressible viscous flows is composed of the Navier-Stokes (N-S) equation

$$\frac{d\mathbf{u}}{dt} = -\frac{1}{\rho}\nabla p + \frac{1}{\rho}(\nabla\mu \cdot \nabla)\mathbf{u} + \mathbf{g}, \quad (1)$$

where  $\rho$  is the density,  $\mathbf{u}$  velocity,  $t$  time,  $p$  pressure,  $\mu$  the dynamic viscosity and  $\mathbf{g}$  an acceleration (gravity in this work); the continuity equation

$$\frac{d\rho}{dt} = -\rho\nabla \cdot \mathbf{u} \xrightarrow{\rho=const} \nabla \cdot \mathbf{u} = 0, \quad (2)$$

and the advection equation (Lagrangian formalism)

$$\frac{d\mathbf{r}}{dt} = \mathbf{u}, \quad (3)$$

where  $\mathbf{r}$  denotes position of the fluid element.

The governing equations can be expressed in the SPH formalism in many different ways. In general, two SPH approximations: integral interpolation and discretization, lead to the the basic SPH relation

$$\langle A \rangle (\mathbf{r}) = \sum_b A(\mathbf{r}_b) W(\mathbf{r} - \mathbf{r}_b, h) \Omega_b, \quad (4)$$

where  $A$  is a physical field (for the sake of simplicity we consider a scalar field only),  $W$  is a weighting function (kernel) with parameter  $h$  called the smoothing length, while  $\Omega$  is the volume of the SPH particle. There are many possibilities for the choice of  $W(\mathbf{r}, h)$ . The kernel shape is the main reason for the appearance of the tensile instability resulting in particle clumping [21] – the process from which the results in [18] suffer. In [22] the authors performed series of fluid-flow simulations and showed that using the Wendland kernel [23] in the form

$$W(\mathbf{r}, h) = C \begin{cases} (1 - q/2)^4 (2q + 1) & \text{for } q \leq 2, \\ 0 & \text{otherwise,} \end{cases} \quad (5)$$

where  $q = |\mathbf{r}|/h$  and the normalization constant is  $C = 7/4\pi h^2$  (in 2D) or  $21/16\pi h^3$  (in 3D), the tensile instability does not appear. Therefore, in this work, we decided to use the kernel in the form of Eq. (5). For more details how the choice of the kernel and the smoothing length affect results see [22]. It is important to note here that the SPH basic approximation, Eq. (4), is common also in other numerical particles-based approaches, e.g. Moving Particle Semi-implicit Method (MPS) [24]. The SPH method differs from other methods in aspect of approximation of differentiation operator. Assuming the kernel symmetry, nabla operator can be shifted from the action on the physical field to the kernel

$$\langle \nabla A \rangle (\mathbf{r}) = \sum_b A(\mathbf{r}_b) \nabla W(\mathbf{r} - \mathbf{r}_b, h) \Omega_b. \quad (6)$$

It is important to note that although different SPH formulations can be obtained from the same governing equations, some of them may not be applicable for certain types of flows, see [25]. One of the most common SPH form, enabling accurate calculations in the widest number of types of flow, is the N-S pressure term proposed by *Colagrossi and Landrini (2003)* [26]

$$\left\langle \frac{\nabla p}{\varrho} \right\rangle_a = - \sum_b m_b \frac{p_a + p_b}{\varrho_a \varrho_b} \nabla_a W_{ab}, \quad (7)$$

where  $\nabla_a W_{ab} = \nabla_a W(\mathbf{r}_a - \mathbf{r}_b, h)$ . In the present work, we decided to perform calculations of pressure term using this variant. The corresponding (variationally consistent [27, 28]) continuity equation takes a form

$$\left\langle \frac{d\varrho}{dt} \right\rangle_a = \varrho_a \sum_b \frac{m_b}{\varrho_b} \mathbf{u}_{ab} \cdot \nabla_a W_{ab}, \quad (8)$$

where  $\mathbf{u}_{ab} = \mathbf{u}_a - \mathbf{u}_b$ . The viscous N-S term, because of the efficiency requirements, is expressed as a combination of the finite difference and the SPH approach (as in the MPS approach [24])

$$\left\langle \frac{1}{\varrho} (\nabla \mu \cdot \nabla) \mathbf{u} \right\rangle_a = \sum_b m_b \frac{\mu_a + \mu_b}{\varrho_a \varrho_b} \frac{\mathbf{r}_{ab} \cdot \nabla_a W_{ab}(h)}{r_{ab}^2 + \eta^2} \mathbf{u}_{ab}, \quad (9)$$

where  $\eta = 0.01h$  is a small regularizing parameter used to avoid *NaNs* when divide by the numerical zero. Because SPH is a Lagrangian approach, the particle advection equation completes the system

$$\frac{d\mathbf{r}_a}{dt} = \mathbf{u}_a. \quad (10)$$

In the present work, we decided to use the most common method of implementing the incompressibility – Weakly Compressible SPH (WCSPH). It involves the set of governing equations closed by a suitably-chosen, artificial equation of state,  $p = p(\varrho)$ . Following the mainstream, we decided to use the Tait’s equation of state

$$p = \frac{c^2 \varrho_0}{\gamma} \left[ \left( \frac{\varrho}{\varrho_0} \right)^\gamma - 1 \right], \quad (11)$$

where  $\varrho_0$  is the initial density. The sound speed  $c$  and a parameter  $\gamma$  are suitably chosen to reduce the density fluctuations down to 1%. In the present work we set  $\gamma = 7$  and  $c$  at the level at least 10 times higher than the maximal fluid velocity. It is worth noting that two alternative incompressibility treatments exists: Incompressible SPH (ISPH) where the incompressibility constraint is explicitly enforced through the pressure correction procedure to satisfy  $\nabla \cdot \mathbf{u} = 0$  [22, 29, 30, 31, 32] and Godunov SPH (GSPH) where the acoustic Riemann solver is used [33]. In the present work, the boundary conditions are fulfilled applying the ghost-particle method [22, 29].

To assure the stability of the SPH scheme several time step criteria must be satisfied:

$$\delta t < 0.125 \frac{h}{c + u_{\max}}, \quad \delta t < 0.125 \frac{\varrho h^2}{\mu_{\max}}, \quad \delta t < 0.125 \left( \frac{h}{g} \right)^{\frac{1}{2}}, \quad (12)$$

where  $u_{\max}$  and  $\mu_{\max}$  are respectively the maximal particle velocity and the maximal particle viscosity in the domain.

### 3 Granular material modeling

In order to simulate the granular materials using the SPH approach, we decided to adopt the visco-plastic rheological model first used in SPH by *Ulrich et al. (2013)* [20]. Equations that predict the shape of the general flow curve need at

least four independent parameters. A common example is the *Cross (1965)* [34] equation

$$\frac{\mu_0 - \mu}{\mu - \mu_\infty} = (K\dot{\gamma})^m, \quad (13)$$

where  $\mu_0$  and  $\mu_\infty$  refer to the asymptotic values of viscosity, while  $K$  and  $m$  are constant. The shear strain rate,  $\dot{\gamma}$ , can be defined as

$$\dot{\gamma} = \sqrt{2\dot{\epsilon}^{ij}\dot{\epsilon}^{ij}}, \quad (14)$$

where

$$\dot{\epsilon}^{ij} = \frac{1}{2} \left( \frac{\partial u^i}{\partial x^j} + \frac{\partial u^j}{\partial x^i} \right). \quad (15)$$

In the case of the granular phase,  $\mu_0$  corresponds to the viscosity of solid (low values of  $\dot{\gamma}$ , elastic limit), while  $\mu_\infty$  is the viscosity of grains above elastic limit (high values of  $\dot{\gamma}$ ). Therefore, we may assume that  $\mu \ll \mu_0$ , which reduces Eq. (13) to the *Sisko (1958)* [35] model

$$\mu = \mu_\infty + \frac{\mu_0}{(K\dot{\gamma})^m} = \mu_\infty + K_2\dot{\gamma}^{n-1}. \quad (16)$$

Assuming  $n = 0$ , we get

$$\mu = \mu_\infty + \frac{K_2}{\dot{\gamma}}, \quad (17)$$

which is commonly known as the *Bingham (1916)* model [36]. With some simple redefinition of parameters Eq. (17) can be written as

$$\tau = \mu_0\dot{\gamma} + \tau_{\text{yield}}, \quad (18)$$

where  $\tau$  is the shear stress,  $\tau_{\text{yield}}$  is the yield stress. In this model, the material behaves as a solid body until the shear stress exceeds the yields stress (reaching the critical state) and large deformations may occur. One of the commonly used models is the Mohr-Coulomb failure criterion [37], in which the shear strength of soil is expressed as a combination of adhesion and friction components

$$\tau_{\text{yield}} = c + \sigma_n \tan \varphi, \quad (19)$$

where  $c$  is the cohesion,  $\varphi$  is the internal friction angle, while  $\sigma_n$  is the normal stress. However, it is important to note that  $c$  and  $\varphi$  are not fundamental properties of material. Both depend on the effective stress [38]. However, for the purposes of the present study, it is sufficiently to assume that  $c$  and  $\varphi$  are fundamental material constants.

Assuming that  $\sigma_n = p$ , the final form of the granular material model takes the form

$$\mu = \begin{cases} \mu_\infty + (c + p \tan \varphi)/\dot{\gamma}, & \mu < \mu_{\text{solid}}, \\ \mu_{\text{solid}}, & \mu \geq \mu_{\text{solid}}, \end{cases} \quad (20)$$

where  $\mu_{\text{solid}}$  is introduced, due to numerical efficiency reasons, to avoid extremely high values of viscosity, which may lead to extremely small time steps (due to CFL).

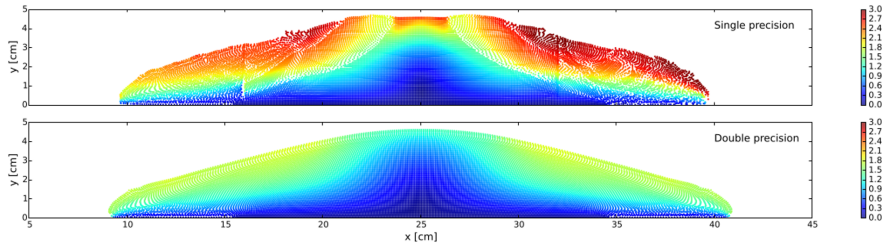


**Fig. 1** 2D granular collapse velocity fields [ $\text{cm s}^{-1}$ ] at  $t = 350$  ( $a = 0.55$  – for details, see Sect. 5.1); the SPH simulations obtained with: (a) single precision and (b) double precision floating point numbers.

#### 4 Graphics Processor Unit implementation

The modern desktop CPUs, such as *Intel i7-4790K*, have 4 physical cores (8 virtual cores via hyper-threading) with the base frequency about 4 GHz. For comparison, the modern desktop GPUs, such as *Nvidia GeForce GTX 980*, have more than  $2 \cdot 10^3$  cores with the base frequency about 1 GHz. Therefore, the advantage of using GPU accelerators for HPC is obvious. The GPU cards were designed to accelerate the creation of images in a frame buffer to stream them onto a display, therefore the double precision was not needed for such a task. Due to this, most of the desktop GPUs are built to support mainly the single precision calculations. There is a possibility to run tasks in double precision, but, it results in a significant drop of performance (officially, for *Nvidia Maxwell series* it is about 16 times). It is important to note that for the most applications of the SPH approach the numerical errors related to the used approximations are much higher than the truncation errors, therefore, many researchers decided to perform the SPH calculations using GPUs with the single precision, see [39, 40, 41, 42]. However, since in our case the kinematic viscosity of a granular material can change the value more than 5 orders of magnitude during a simulation, the single precision is not enough. The influence of the floating point number precision on the results is presented in Fig. 1.

The problem of the double precision floating point numbers in the SPH modeling on GPU has been recently discussed in [43] and [44]. To avoid this problem the authors proposed to use such techniques as the cell relative coordinates (to avoid problems in domains of high aspect ratios) or the compensated algorithms like Kahan sum (to sum over large numbers of values). Unfortunately, none of the proposed algorithms could correct the problem of strongly inhomogeneous viscosity in domain. Therefore, in the present work, to avoid inaccuracies, we decided to perform calculations using the double precision explicitly. The influence on the numerical efficiency is discussed in Section 5.6. For details about the GPU implementation see [40].

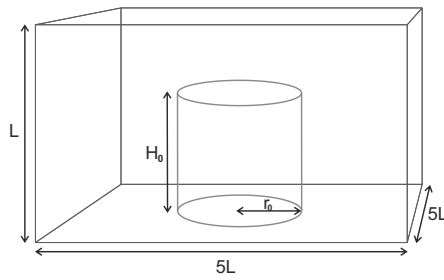


**Fig. 2** Initial configuration in 3D.

## 5 Numerical results

### 5.1 Introduction

The numerical experiments were performed by releasing initially vertical columns of granular material, see Fig. 2. The initial height,  $H_0$ , was defined by the initial radius  $r_0 = 9.7$  cm and the aspect ratio parameter

$$a = \frac{H_0}{r_0}. \quad (21)$$

The material density  $\rho$  was  $2.6 \text{ g cm}^{-3}$ . The angle of repose  $\varphi$  was  $30^\circ$  (except Section 5.5). The material was chosen as non-cohesive,  $c = 0$ . These are properties of dry sand used in the experiment of *Lube et al. (2004)* [45]. Initially the granular column is placed in the middle of the base of the rectangular domain of edges  $(5L, 5L, L)$  in 3D or  $(5L, L)$  in 2D, where  $L = 1.8H_0$  is the domain height. For  $a < 0.9$  we have chosen  $L = 10$  cm, while for others  $L = 1.2H_0$ .

The SPH simulations were performed for different aspect ratios and different numerical resolutions. In 2D:  $a = 0-10$ ,  $h/L = 16-64$  and  $h/\Delta r = 2$ . In 3D:  $a = 0-6$ ,  $h/L = 16-64$  and  $h/\Delta r = 1.5625$  (lower than 2D due to the efficiency reasons). In both cases, we decided to use the Wendland kernel (to avoid problems with the tensile instability). The speed of sound was  $s = 1000 \text{ cm s}^{-1}$ . The parameter  $\mu_\infty$  in Eq. (20) was chosen as a viscosity of water (at  $20^\circ\text{C}$ ),  $0.01 \text{ g cm}^{-1} \text{ s}^{-1}$ . The viscosity of solid  $\mu_{\text{solid}}$  was chosen as  $2000 \text{ g cm}^{-1} \text{ s}^{-1}$ . Due to the efficiency reasons, see Eq. (12), the value of  $\mu_{\text{solid}}$  is suitably lowered compared with the real soil. The side effects of such proceedings are negligible. The calculations were performed using the double precision floating point number with the single precision calculations used only to benchmark the numerical efficiency in Section 5.6.

### 5.2 Shape evolution

The simplest technique to check whether the proposed model gives the correct results is to compare the calculated profile shapes with other numerical and



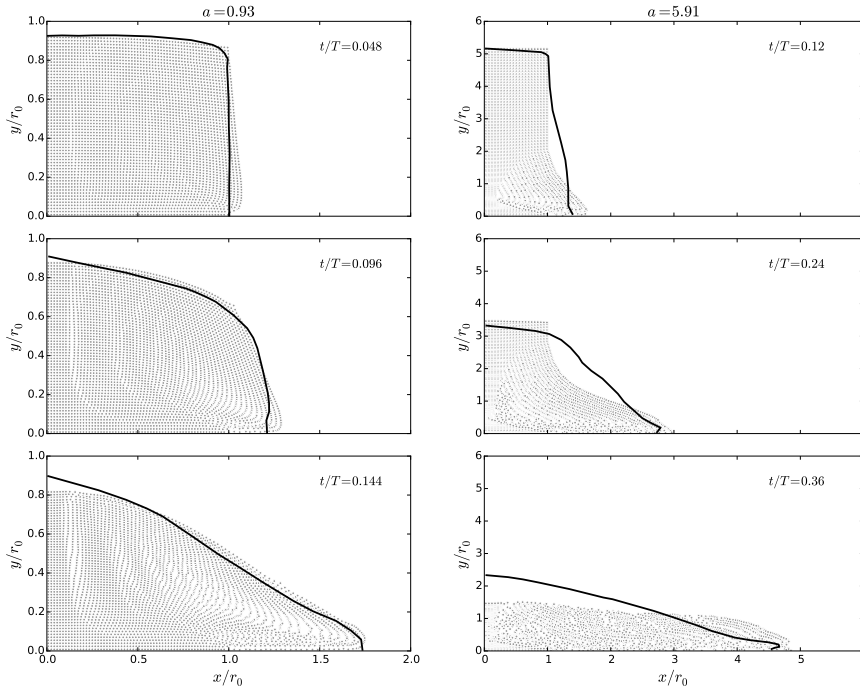


**Fig. 3** The evaluation of profiles for different initial aspect ratios,  $a$ , of granular columns (2D); the SPH results compared with the DEM reference data [12] (solid lines).

experimental data. In 2D, as a reference data we decided to choose the DEM calculations obtained by *Uttili et al. (2015)* [12]. The obtained results, for aspect ratios:  $a = 0.93$  and  $a = 5.91$ , are presented in Fig. 3. For  $a = 0.93$  the SPH results show good agreement with the reference data. In the case of higher aspect ratio,  $a = 5.91$ , the SPH calculations slightly differ from the DEM calculations – mainly the final height of the sample.

For the 3D model, it was decided to compare the SPH results with the experimental data by *Lube et al. (2004)* [45]. For validation purposes we have chosen two different aspect ratios:  $a = 0.55$  and  $a = 2.75$ . The results are presented in Fig. 4. The performed simulations gave very realistic results. Using the SPH approach, we were able to reproduce the typical for  $a < 0.74$ , see [45], circular discontinuity on the surface of the column which separates an outer (slumping) region from a non-deformed inner part of the deposit. For the column of  $a = 2.75$  the calculated shape evolution of the column agrees very well with the experimental data presented in detail in [45] (Figure 4).

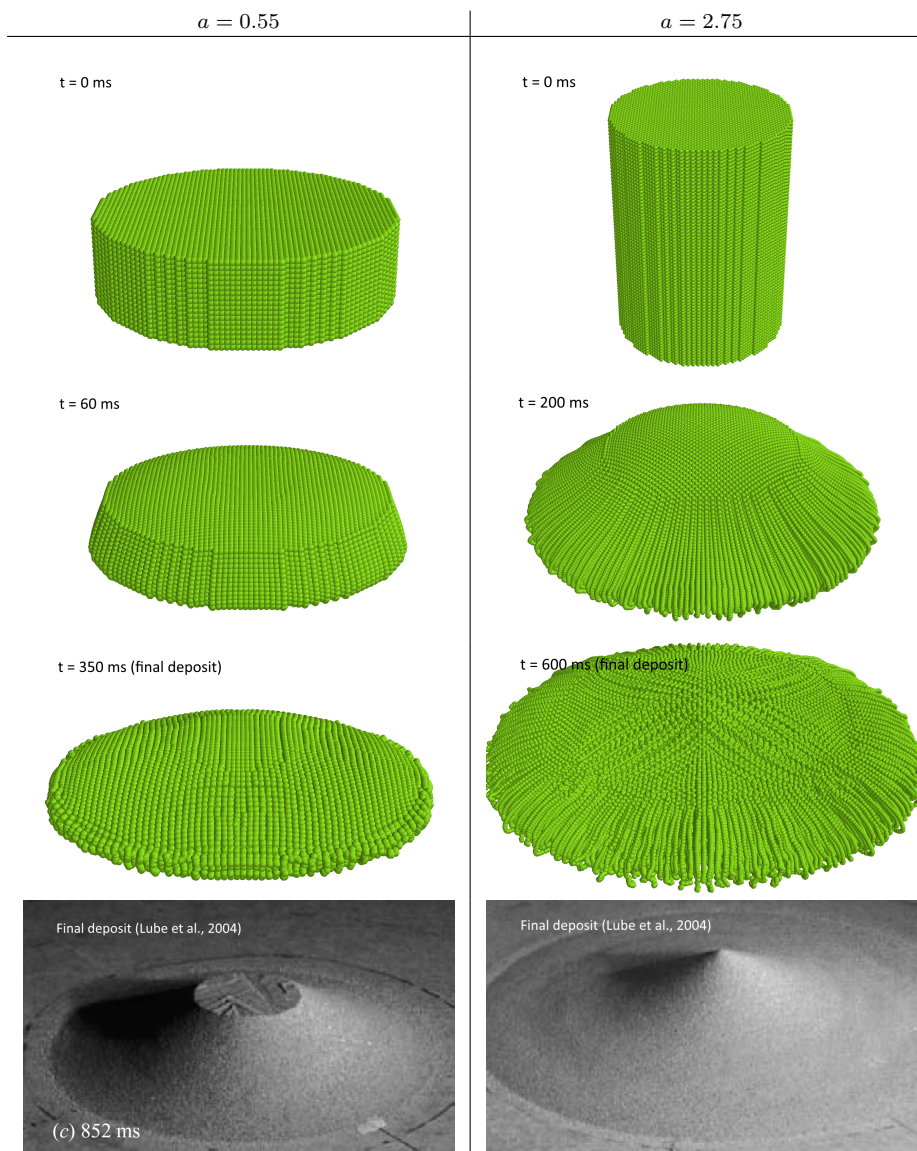


**Fig. 4** The evolution of granular material column for different initial aspect ratios:  $a = 0.55$  and  $2.75$ ; the SPH results compared with the experimental photographs by *Lube et al. (2004)* [45].

### 5.3 Run-out distances

One of the most relevant validation criteria for the numerical model is to try to reproduce the scaling laws for the run-out distance. The experimental data

for the three-dimensional column was first proposed by *Lube et al. (2004)* [45]:

$$\frac{r_\infty - r_0}{r_0} \simeq \begin{cases} 1.24a, & a < 1.7, \\ 1.6a^{1/2}, & a \geq 1.7. \end{cases} \quad (22)$$

Slightly different results were obtained by *Lajeunesse et al. (2005)* [5] for semi-circular (half of column) initial configuration:

$$\frac{r_\infty - r_0}{r_0} \simeq \begin{cases} a, & a < 3, \\ a^{1/2}, & a \geq 3. \end{cases} \quad (23)$$

Many more empirical and numerical experiments were performed for granular collapses of the two-dimensional columns. *Lube et al. (2005)* [46] were releasing a granular columns confined between two vertical walls. The authors obtained the following scaling:

$$\frac{r_\infty - r_0}{r_0} \simeq \begin{cases} 1.2a, & a < 2.3, \\ 1.9a^{2/3}, & a \geq 2.3. \end{cases} \quad (24)$$

Independently *Lajeunesse et al. (2005)* obtained a similar result:

$$\frac{r_\infty - r_0}{r_0} \simeq \begin{cases} a, & a < 3, \\ a^{2/3}, & a \geq 3. \end{cases} \quad (25)$$

The two-dimensional numerical experiments were performed by *Staron and Hinch (2005)* [8] who obtained the relation:

$$\frac{r_\infty - r_0}{r_0} \simeq \begin{cases} 2.5a, & a < 2, \\ 3.25a^{0.7}, & a \geq 2. \end{cases} \quad (26)$$

Many other authors including *Zenit (2005)* [11], *Uttili et al. (2015)* [12] who used the DEM approach and *Crosta et al. (2009)* [14] who performed FEM simulations obtained fairly consistent results for the run-out distance.

The obtained results of the relation between the normalized run-out distance and the initial column aspect ratio for 2D and 3D cases are respectively presented in Figs. 5 and 6. As the reference data we decided to plot two- and three-dimensional experimental solution obtained in *Lube et al. [46,45]*.

Here we show that in the case of 2D columns the normalized run-out distances for higher aspect ratios are slightly overestimated when compared with the experimental data [46]. In the present SPH approach, we obtained:

$$\frac{r_\infty - r_0}{r_0} \simeq \begin{cases} 1.3a, & a < 2, \\ 1.55a^{4/5}, & a \geq 2. \end{cases} \quad (27)$$

However, in general, the results show a good agreement with the reference data.

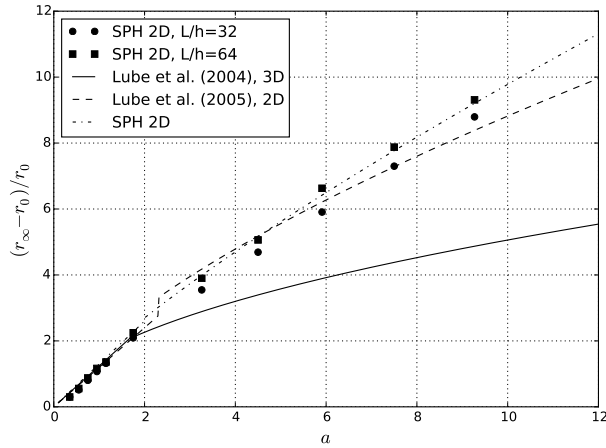


**Fig. 5** The non-dimensional incremental run-out distance as a function of the aspect ratio for two-dimensional results; the SPH solution compared with two- [46] and three-dimensional [45] experimental data.

In the case of 3D columns, we obtained somewhat less accurate results compared with the reference data [45]. The SPH results appear to be underestimated. One reason of such a behavior is smaller numerical resolution compared with the 2D simulations. The obtained scaling law is:

$$\frac{r_\infty - r_0}{r_0} \simeq \begin{cases} 0.85a, & a < 1.7, \\ 1.05a^{3/5}, & a \geq 1.7. \end{cases} \quad (28)$$

#### 5.4 Energy contribution

The potential energy of the column at any time is

$$E_p = \sum_a m_a g h_a, \quad (29)$$

where  $h_a$  is the height of the particle  $a$ . The column kinetic energy can be calculated from

$$E_k = \frac{1}{2} \sum_a m_a u_a^2. \quad (30)$$

Due to the viscosity, or (in the scale of a single grain) non-elastic collisions between grains, a part of the potential energy does not transform into the kinetic energy, but it gets dissipated

$$E_{dis}(t) = E_p(0) - E_p(t) - E_k(t). \quad (31)$$

At the beginning, the entire energy is accumulated as the potential energy. As time passes, particles start to fall downwards with the potential energy

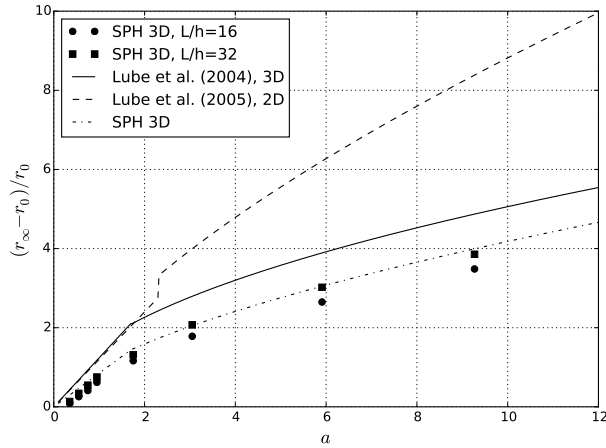


**Fig. 6** The non-dimensional incremental run-out distance as a function of the aspect ratio for three-dimensional results; the SPH solution compared with two- [46] and three-dimensional [45] experimental data.

being transformed into the kinetic energy and some heat (dissipation). Figure 7(left) shows the energy evolution of the granular column for the aspect ratio  $a = 3.26$ . In this plot the SPH results are compared with the DEM simulations obtained in [12]. In both models the kinetic energy exhibits a peak at about  $t/T = 1$ . The obtained results show small discrepancies between SPH and DEM, however these differences can be minimized adjusting the minimal and maximal viscosity in the considered rheological model.

In order to validate the SPH approach for different values of the aspect ratio, we decided to compare the total dissipated energy for different values of  $a$  calculated using the SPH method with the DEM simulations [12]. The obtained results are presented in Fig. 7(right). Both SPH and DEM models give similar relation between the dissipated energy and aspect ratio. Small overestimation of the SPH results is also observed in Fig. 7(left).

### 5.5 Inclination of the failure plane

According to the Rankine's theory of earth pressure [47], the inclination of the failure plane to the horizontal,  $\theta_f$  can be approximated as:

$$\theta_f = 45^\circ + \frac{\varphi}{2}. \quad (32)$$

In order to check whether the SPH approach can correctly predict the relation (32), we decided to perform three simulations of granular column collapse with different values of the internal friction angle  $\varphi = 20^\circ$ ,  $30^\circ$ , and  $40^\circ$ . It is important to note that values  $20^\circ$  and  $40^\circ$  correspond to the extreme values observed in nature. To visualize the inclination angle of the slope failure plane,

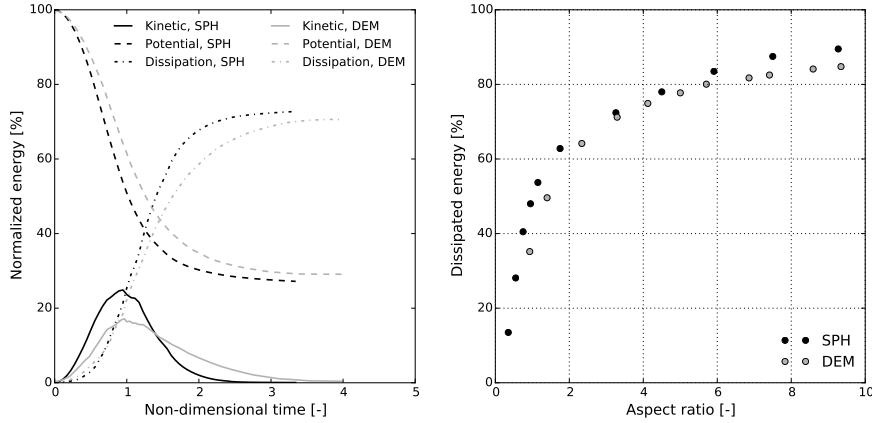


**Fig. 7** (left) Energy evolution for the granular column of the aspect ratio  $a = 3.26$ ; (right) total energy dissipated during the flow as a function of the aspect ratio; energy normalized by the initial potential energy; the SPH result compared with the DEM reference data [12].

we decided to plot the velocity fields using the spectral color map, see Fig. 8. The presented results were obtained for the collapsing column of aspect ratio  $a = 0.55$  at  $t = 40$  ms. The obtained failure angles agree well with the relation (32). Similar test performed for different values of aspect ratios show no vital differences in relation between  $\theta_f$  and  $\varphi$ . The only problem that must be noted is small systematic decline of the  $\theta_f$  values for vary late time steps. This behavior is due to decrease of the height of the deposit caused by lowered  $\mu_{\text{solid}}$  (compared with reality) due to the numerical efficiency, see Section (5.1).

## 5.6 Numerical efficiency

For the performance analysis we decided to use the *Nvidia GeForce GTX980* GPU (2048 cores, 1126 MHz clock, 4 GB of memory). Figure 9 presents the measured Frames (time steps) Per Second (FPS) as a function of the number of particles in the domain. In 2D, the use of the double precision floating numbers decreases the computational time twice. In single precision the calculations took from about 2 min for about  $N = 4 \cdot 10^3$  particles up to about 1 h for  $N = 2.5 \cdot 10^5$ . In 3D, the use of the single precision numbers increases performance by factor 3. For the lowest used resolution ( $N = 2.5 \cdot 10^4$ ) simulations took 23 min, while for the highest resolution ( $N = 1.5 \cdot 10^6$ ) about 26 h (single precision). It is important to note that the used GPU is based on the *Maxwell* micro-architecture in which the double precision performance is 1/32 of the single precision performance. Therefore, the main reason of observed decrease of the performance with double precision in 3D (compared with the single precision) is much larger number of interactions under the kernel hat (larger number of simple math operations). The difference between the double and single precision performance should be much smaller using the *Kepler* micro-

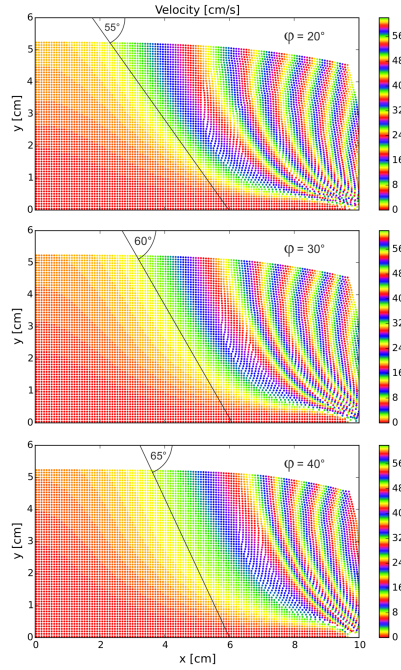


**Fig. 8** Active failure state of the granular sample; the results obtained for three different internal friction angles: (a)  $20^\circ$ , (b)  $30^\circ$  and (c)  $40^\circ$ .

architecture (*Nvidia Tesla* and *Nvidia GeForce 700 series*) where the double precision computations are only 4 times less efficient. The numerical efficiency can be further improved by using more than one GPU.

## 6 Conclusions

In the present work, the ability to model granular materials using the SPH method and the visco-plastic model has been studied. For this purpose, a set of numerical calculations (in 2D and 3D) of the fundamental problem of the collapse of initially vertical cylinders of granular materials has been performed. In order to validate the proposed model, the granular deposit evolution, the run-out distances, the energy contribution and the inclination of the failure plane were compared with the analytical, experimental and other numerical data. The obtained results showed good agreement with the reference data. All the inaccuracies that we observed during simulations were caused mainly by two factors: not perfectly matched parameters of the used rheological model or too low numerical resolution (limited hardware resources). In order to reduce the effect of particle clustering (the tensile instability) – the problem signalized in [18], we decided to suitably choose the kernel function which significantly reduces this problem. In fact, the tensile instability was not observed

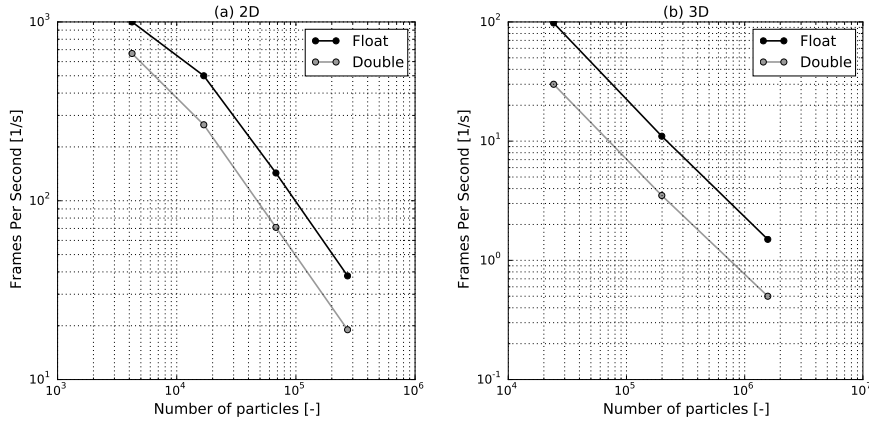


**Fig. 9** Number of frames per second as a function of the SPH particles in the domain; the initial aspect ratio is  $a = 0.55$ ; (a) two-dimensional results for  $h/\Delta r = 2$ , (b) three-dimensional results for  $h/\Delta r = 1.5625$ .

in the obtained results. Taking advantage of GPU efficiency, it was possible to run computationally heavy simulations on the cheap desktop computer. The performed analysis showed that the single precision of floats is not enough to correctly perform simulations with the used rheological model. The double precision calculations increase the computational effort on GPU, but, the obtained numerical efficiency is still very high. It is important to note here that for dry granular materials the methods such as the DEM allow for much more accurate and efficient calculations. However, when we consider complex debris flow constituted of rocks and mud, for which it may be difficult to define the interaction between solid particles, the continuum methods, such as the introduced SPH, appear to be much more useful. Another advantage of the SPH approach is its ability to model complex multi-phase flows involving eg. fluid-granular phase interactions. This work is an intermediate step in a complete project which aims at simulating the interaction of sea waves and currents with a seabed. The satisfactory results obtained for the dynamics of dry sand with the simple rheological model are an encouragement to pursue along that direction.

## Funding

This study was funded by the National Science Centre, Poland via grant Opus 6 no DEC-2013/11/B/ST8/03818.

## Conflict of Interest

The author declare that he has no conflict of interest.



## References

1. S.B. Savage, K. Hutter, The motion of a finite mass of granular media down a rough incline, *J. Fluid Mech.* 199 (1989) 177-215.
2. K.G. Anderson, R. Jackson, A comparison of the solutions of some proposed equations of motion of granular materials for fully developed flow down inclined planes, *J. Fluid Mech.* 241 (1992) 145-168.
3. O. Poliquen, Scaling laws in granular flows down rough inclined planes, *Phys. Fluids* 11 (1999) 542-548.
4. R.M. Iverson, R.P. Denlinger, Flow of variably fluidized granular masses across three-dimensional terrain. Part I: Coulumb mixture theory, *J. Geophys. Res.* 106 (2001) 537-552.
5. E. Lajeunesse, J.B. Monnier, G.M. Homsy, Granular slumping on a horizontal surface, *Phys. Fluids* 17 (2005) 103302.
6. P.A. Cundall, O.D.L. Strack, A discrete numerical model for granular assemblies, *Geotechnique* 29 (1979) 47-65.
7. P.W. Cleary, C.S. Campbell, Self-lubrication for long runout landslides: examination by computer simulation, *J. Geophys. Res. Solid Earth* 98 (1993) 21911-21924.
8. L. Staron, E.J. Hinch, Study of the collapse of granular columns using DEM numerical simulation, *J. Fluid Mech.* 545 (2005) 1-27.
9. L. Staron, E.J. Hinch, The spreading of a granular mass: role of grain properties and initial conditions, *Granul. Matter* 9 (2007) 205-217.
10. C.L. Tang, J.C. Hu, M.L. Lin, J. Angelier, C.Y. Lu, Y.C. Chan, H.T. Chu, The Tsaoling landslide triggered by the Chi-Chi earthquake, Taiwan: insights from a discrete element simulation, *Eng. Geol.* 106 (2009) 1-19.
11. R. Zenit, Computer simulations of the collapse of a granular column, *Phys. Fluids* 17 (2005) 1-4.
12. S. Utili, T. Zhao, G.T. Houlsby, 3D DEM investigation of granular column collapse: Evaluation of debris motion and its destructive power, *Eng. Geol.* 186 (2015) 3-16.
13. O.C. Zienkiewicz, R.L. Taylor, J.Z. Zhu, *The Finite Element Method: Its Basis and Fundamentals* (Sixth ed.), Butterworth-Heinemann 2005.
14. G.B. Crosta, S. Imposimato, D. Roddeman, Numerical modeling of 2-D granular step collapse on erodible and nonerodible surface, *J. Geophys. Res.* 114 (2009) F03020.
15. J.J. Monaghan, Smoothed Particle Hydrodynamics, *Annu. Rev. Astron. Astr.* 30 (1992) 543-574.
16. J.J. Monaghan, Smoothed Particle Hydrodynamics and its diverse applications, *Annu. Rev. Fluid Mech.* 44 (2012) 323-346.
17. D. Violeau, *Fluid Mechanics and the SPH Method: Theory and Applications*, Oxford University Press, 2012.
18. H.H. Bui, R. Fukagawa, K. Sako, S. Ohno, Lagrangian meshfree particles method (SPH) for large deformation and failure flows of geomaterial using elastic-plastic soil constitutive model, *Int. J. Numer. Anal. Meth. Geomech.* 32 (2008) 1537-1570.
19. H.H. Bui, J.K. Kodikara, A. Bouazza, A. Haque, P.G. Ranjith, A novel computational approach for large deformation and post-failure analyses of segmental retaining wall systems, *Int. J. Numer. Anal. Meth. Geomech.* 38 (2014) 1321-1340.
20. C. Ulrich, M. Leonardi, T. Rung, Multi-physics SPH simulation of complex marine-engineering hydrodynamic problems, *Ocean Eng.* 64 (2013) 109-121.
21. J.W. Swegle, D.L. Hicks, S.W. Attaway, Smoothed Particle Hydrodynamics stability analysis, *J. Comput. Phys.* 116 (1995) 123-134.
22. K. Szewc, J. Pozorski, J.P. Minier, Analysis of the incompressibility constraint in the SPH method, *Int. J. Num. Meth. Eng.* 92 (2012) 343-369.
23. H. Wendland, Piecewise polynomial, positive definite and compactly supported radial functions of minimal degree. *Adv. Comp. Math.* 4 (1995) 389-396.
24. S. Koshizuka, A. Nobe, Y. Oka, Numerical analysis of breaking waves using the moving particle semi-implicit method, *Int. J. Num. Meth. Fl.* 26 (1998) 751-769.
25. K. Szewc, A. Tanière, J. Pozorski, J.P. Minier, A study on application of smoothed particle hydrodynamics to multi-phase flows, *Int. J. Nonlin. Sci. Num. Sim.* 13 (2012) 383-395.

26. A. Colagrossi, M. Landrini, Numerical simulation of interfacial flows by smoothed particle hydrodynamics, *J. Comput. Phys.* 191 (2003) 227-264.
27. N. Grenier, M. Antuono, A. Colagrossi, D. Le Touzé, B. Allessandrini, An Hamiltonian interface SPH formulation for multi-fluid and free-surface flows, *J. Comput. Phys.* 228 (2009) 8380-8393.
28. J.J. Monaghan, Smoothed particle hydrodynamics. *Rep. Prog. Phys.* 68 (2005) 1703-1759.
29. S. Cummins, M. Rudman, An SPH projection method, *J. Comput. Phys.* 152 (1999) 584-607.
30. X.Y. Hu, N.A. Adams, An incompressible multi-phase sph method, *J. Comput. Phys.* 227 (2007) 264-278.
31. S. Shao, E.Y.M. Lo, Incompressible SPH method for simulating Newtonian and non-Newtonian flows with a free surface, *Adv. Water Res.* 26 (2003) 787-800.
32. R. Xu, P. Stansby, D. Laurence, Accuracy and stability in incompressible sph based on the projection method and a new approach, *J. Comput. Phys.* 228 (2009) 6703-6725.
33. A. Rafiee, S. Cummins, M. Rudman, K. Thiagarajan, Comparative study on the accuracy and stability of SPH schemes in simulating energetic free-surface flows, *Eur. J. Mech. B-Fluid* 36 (2012) 1-16.
34. M.M. Cross, Rheology of non-Newtonian fluids: a new flow equation for pseudo-plastic systems, *J. Colloid Sci.* 20 (1965) 417-437.
35. A.W. Sisko, The flow of lubricating greases, *Ind. En. Chem.* 50 (1958) 1789-1792.
36. E.C. Bingham An investigation of the laws of plastic flow, U.S. Bureau of Standards Bulletin 13 (1916) 309-353.
37. C.A. Coulumb, Essai sur une application des regles des maximis et minimis a quelques problemes de statique relatifs, a la architecture, *Mem. Acad. Roy. Div. Sav.* 7 (1776) 343-387.
38. T.W. Lambe, R.V. Whitman, *Soil Mechanics*, Wiley, 1991.
39. A. Hérault, G. Bilotta, R.A. Dalrymple, SPH on GPU with CUDA, *J. Hydraul. Res.* 48 (2010) 74-79.
40. K. Szewc, Smoothed Particle Hydrodynamics simulations using Graphics Processing Units, *TASK Quarterly* 18 (2014) 67-80.
41. E. Rustico, J. Jankowski, A. Hérault, G. Bilotta, C.D. Del Negro, Mluti-GPU, multi-node SPH implementation with arbitrary domain decomposition, *Proceedings of the 9th SPHERIC International Workshop*, Paris, 2014.
42. A.J.C. Crespo, J.M. Domínguez, B.D. Rogers, M. Gómez-Gesteira, S. Longshaw, R. Canelas, R. Vacondio, A. Barreiro, O. García-Feal, DualSPHysics: Open-source parallel CFD solver based on Smoothed Particle Hydrodynamics (SPH), *Comp. Phys. Comm.* 187 (2015) 204-216.
43. A. Hérault, G. Bilotta, R.A. Dalrymple, Achieving the best accuracy in an SPH implementation, *Proceedings of the 9th SPHERIC International Workshop*, Paris, 2014.
44. J.M. Domínguez, A.J.C. Crespo, A. Barreiro M. Gómez-Gesteira, B.D. Rogers, Efficient implementation of double precision in GPU computing to simulate realistic cases with high resolution, *Proceedings of the 9th SPHERIC International Workshop*, Paris, 2014.
45. G. Lube, H.E. Huppert, S.S. Sparks, M.A. Hallworth, Axisymmetric collapses of granular columns, *J. Fluid Mech.* 508 (2004) 175-199.
46. G. Lube, H.E. Huppert, S.S. Sparks, A. Freundt, Collapses of two-dimensional granular columns, *Phys. Rev. E* 72 (2005) 041301.
47. W.J.M. Rankine, On stability of loose earth, *Philos. Trans. R. Soc. Lond.* 147 (1857) 9-27.